The crystal structure of sacrofanite, the 74 Å phase of the cancrinite–sodalite supergroup

The crystal structure of sacrofanite,

the 74 Å phase of the cancrinite-sodalite supergroup

Bonaccorsi E.[a,*], Ballirano P.[b,c], Cámara F.[d,e]

[a] Dipartimento di Scienze della Terra, University of Pisa - Via S. Maria 53, I-56126 Pisa, Italy

[b] Dipartimento di Scienze della Terra, Sapienza University of Roma - Piazzale A. Moro 5, I-00185 Roma, Italy

[c] CNR-IGAG, Istituto di Geologia Ambientale e Geoingegneria, - Via Bolognola 7, I-00138 Roma, Italy

[d] Dipartimento di Scienze Mineralogiche e Petrologiche, University of Torino - Via Valperga Caluso 35, I-10125 Torino, Italy

[e] CNR-IGG, Istituto di Geoscienze e Georisorse, via Ferrata 1, I-27100 Pavia, Italy

* Corresponding author:

Elena Bonaccorsi

Dipartimento di Scienze della Terra, University of Pisa - Via S. Maria 5 I-56126 Pisa, Italy

Tel. +39 050 2215704

Fax +39 050 2215830

E-mail address: elena@dst.unipi.it

Abstract

Sacrofanite, a = 12.903(2) Å, c = 74.284(8) Å, space group $P\bar{6}2c$, belongs to the cancrinite-sodalite supergroup of minerals, and displays a 28-layer stacking sequence along the c axis. Its stacking sequence is ABCABACACABACBACBACABABACABC... , where A, B and C stand for the positions of six-member rings of tetrahedra in each layer. It corresponds to the Zhdanov symbol |12(8)21|12(8)21|, and gives rise to a framework with topological symmetry $P6_3/mmc$. The ordering of Si and Al in the tetrahedral sites reduces the symmetry to $P\bar{6}2c$. The members of this supergroup of minerals belong to the wider ABC-6 family, where also double rings of tetrahedra may occur. They share many structural features with zeolites, showing structural cages hosting extra-framework ions as well as H_2O molecules. The crystal structure of sacrofanite has been modeled on the basis of High Resolution Transmission Electron Microscopy (HRTEM) images. The resulting model has been successfully refined by using both single-crystal synchrotron radiation and laboratory data. The refinements converged to R = 0.083 for 4,228 unique reflections, and to R = 0.096 for 15,795 unique reflections, respectively. The resulting framework is formed by eight cancrinite and four sodalite cages superimposed along [0, 0, z], whereas one cancrinite, four sodalite, two losod, and one liottite cages occur along [1/3, 2/3, z] and [2/3, 1/3, z]. The structural formula of sacrofanite, as obtained from the refinement and by crystal chemical considerations, is $(Na_{61}K_{19}Ca_{32})_{\Sigma=112}(Si_{84}Al_{84}O_{336})(SO_4)_{26}Cl_2F_6 \cdot 2H_2O$.

Key-words: sacrofanite, cancrinite-sodalite supergroup, cages, ABC-6 family, HRTEM

1. Introduction

The main features of the minerals belonging to the group up to now known as ‘cancrinite group’ or 'cancrinite-sodalite group' were recently reviewed [1, 2]. Their frameworks are characterised by layers containing six-membered rings of tetrahedra, with each ring being linked to three similar rings in the preceding layer and to three rings in the succeeding one. If the position of the rings in the first layer is labelled “A”, and the two possible alternative positions in the adjacent layers are “B” and “C”, following the notation of the closest-packed structures, the resulting framework can be described by a sequence of A, B, C symbols, without repetition of letters. These minerals constitute a minor division of the wider ‘ABC-6 family’ [3], which includes also natural and synthetic microporous phases with double six-membered rings (for example chabazite, with sequence AABBCC), possibly mixed with layers of single rings. All the phases that show only single six-membered rings could be indeed considered a supergroup, in accordance with the definition of [4]. This supergroup includes several different groups characterised by distinct stacking sequences of the layers: the ‘sodalite group’ (ABC) and ‘cancrinite group’ (AB) are the most known among them. The quite recent discovery of alloriite [5], with the same stacking sequence of afghanite, could point to the new ‘afghanite group’ (two phases with ABABACAC stacking sequence but different composition). In the same way, bystrite and the recently defined new mineral carbobystrite [6], which displays the same stacking sequence ABAC, should form a new ‘bystrite group’. On the contrary, marinellite and tounkite, which display the same number of layers (12) but different stacking sequences and therefore different structure, do not form a separate mineral group. The last consideration holds also for franzinite and a recently described natural

'ten-layer phase' [7], which display a different stacking sequence. A scheme of this classification is reported in Table 1.

The useful description of the minerals belonging to the cancrinite-sodalite supergroup as due to the different stacking of layers A, B and C does not mean at all that they are polytypes of cancrinite or sodalite, at difference from what happens in the closest-packed structures. This simplified description refers only to the framework topology, as the nature and position of the extra-framework atoms greatly depend on the size and number of the available cages.

So far, sacrofanite was found only in the type locality, namely Sacrofano, Latium, Italy [8]. According to the authors, its chemical formula, based on 12(Si+Al) atoms, is $(Na_{6.25}K_{1.39}\ Ca_{1.83})_{\Sigma 9.47}(Si_{6.26}Al_{5.74})_{\Sigma 12.00}O_{24}(OH)_{2.69}(SO_4)_{1.14}(CO_3)_{0.27}Cl_{0.20} \cdot 0.27H_2O$, space group $P6_3/mmc$, $P6_3mc$ or $P\bar{6}2c$, with unit cell parameters a = 12.865 Å, c = 72.240 Å.

A sample from the same locality was successively studied [9] and a new chemical formula based on 12(Si+Al) was proposed: $(Na_{3.75}K_{1.65}Ca_{2.31})_{\Sigma 7.73}(Si_{6.04}Al_{5.96})_{\Sigma 12.00}O_{23.96}(SO_4)_{1.84}Cl_{0.17}F_{0.29} \cdot nH_2O$[1]. At difference from the old data, here the sum of the extra-framework cations is close to 8, which is the ideal value, and fluorine was detected among the extra-framework anions.

Sacrofanite displays one of the longest sequences of layers in this supergroup, corresponding to 28 layers. Only three other recently described members of the supergroup, namely biachellaite [10], fantappieite [11, 12] and kircherite [13] have longer c parameters, being formed, respectively, by 30 layers (c = 79.6 Å), by 11×3

[1] Recalculation from the original data showed, a part of small rounding errors, a misprint in the chemical formula as the populations of Cl and F have to be exchanged.

layers in a rhombohedral centred cell with c = 87.2 Å, and by 12×3 layers in a rhombohedral centred cell, with c = 95.2 Å.

The determination of the correct stacking sequence of sacrofanite was complicated by its huge unit cell; from a theoretical point of view more than 8×10^5 non equivalent stacking sequences are possible, prohibiting a trial-and-error strategy. Different approaches were tried, and finally its stacking sequence was determined by means of high-resolution transmission electron microscopy (HRTEM) images. The model was confirmed by single crystal structural refinement against synchrotron radiation [14] and, successively, laboratory CCD-detected data. Both the transmission electron microscopy results and the structural refinements are presented in the following paragraphs.

2. Experimental

2.1 Structural model by HRTEM images

The HRTEM study was carried out on a JEOL 4000EX TEM, equipped with a top-entry double-tilt (± 30°) goniometer stage, operated at an accelerating voltage of 400 kV. A fragment of a crystal of the sacrofanite sample MMUR 24320 (from the collection of the Mineralogical Museum of the University of Roma), previously characterised [9], was crushed in a mortar. The resulting powder was dispersed in ethanol into a beaker and treated for 10 minutes with an ultrasonic cleaner. A small drop of the dispersion was deposited onto a carbon-coated copper grid. Images recorded on thin areas near the edge of the crystal were digitised by a scanner and evaluated by Crystallographic Image Processing, CIP [15], using the CRISP software [16]. In particular an HRTEM image (Fig. 1), taken along [100] and showing the stacking sequence of sacrofanite, was selected for CIP. The Fourier transform of a 512 x 512

pixel area was calculated and the absence of an elliptical dark ring arising from Contrast Transfer Function (CTF) crossover indicated that the image was properly taken at the Scherzer-focus condition. The lattice was refined and amplitudes and phases were extracted. The symmetry of the 17 plane-groups was therefore successively tried, together with different choices of the origin. A list of figures of merit, in the form of *R*-values for amplitudes (R_A%) and Phase residuals on phases (R_P°), was finally obtained. The lowest values for R_P (and R_A) were obtained for the plane groups $p12_1$ ($p1g1$ = 10°), $p22_12$ ($p2gm$ = 25°), and $p22_12_1$ ($p2gg$ = 25°), respectively.

Reference data [8] indicate $P6_3/mmc$, $P6_3mc$, and $P\bar{6}2c$ as possible space groups of sacrofanite: along [100] they show planar symmetry $p2gm$, $p1g1$, and $p2gm$ respectively. This fact allowed us to discard $p2gg$ as a possible correct symmetry for our image. After implementation of the two remaining symmetries, images of the potential maps were calculated showing extremely slight differences between them.

Inspection of the maps revealed the stacking sequence of sacrofanite as ABACABCABCABACACABACBACBACAB, Zhdanov symbol |12(8)21|12(8)21|. Following the subunits model proposed in [17], this sequence leads to 8 cancrinite and 4 sodalite cages along A, 1 cancrinite, 4 sodalite, 2 losod, and 1 liottite cages along B and C, for a total of 12 sodalite, 10 cancrinite, 4 losod, and 2 liottite cages (Fig. 3).

2.2 X-ray data collections

Two data collections were performed, on two selected crystals from the same locality. The former was performed at the XRD1 beamline of the Elettra synchrotron radiation facility. A single crystal of sacrofanite with dimensions $0.2 \times 0.1 \times 0.1$ mm^3, coming from the same specimen examined during the HRTEM study and previously analysed [9], was irradiated with a monochromated X-ray beam, nominal wavelength λ

= 1.0 Å, and at a distance of 40 mm from a 165mm Mar CCD detector. The crystal was rotated around the φ axis, and 360 frames were collected, giving rise to 78,202 observed reflections. The reflections were indexed, integrated and scaled by means of the programs Xdisp, Denzo and Scalepack [18]. The intensity set appeared of good quality (R_{int} = 3.5 %), and it was sufficient to refine the structure of sacrofanite, confirming the framework model suggested by HRTEM [14]. However, the experimental setting did not allow data to be collected at higher resolution. To overcome this limit, an additional data collection was performed with a Bruker-AXS single-crystal diffractometer with a SMART-APEX CCD detector (Mo-*K*α radiation), and a collimator with a diameter of 0.8 mm. The data collection was performed on a crystal of sacrofanite coming from a sample of the mineral collection of F.S. Stoppani, kindly given us by Dr. Fabio Bellatreccia. The detector-to crystal working distance was 8 cm. The data were corrected for the Lorentz and polarization factors and an empirical absorption correction (SADABS, [19]) was applied. The refined unit cell parameters were obtained from 8820 reflections with $I < 10\sigma(I)$ collected in the 2θ range 5-70º. Ten data sets of 900 images were collected for 5 seconds performing 0.2° ω-scans at different ϕ angles (0, 90, 180 and 270° with the detector at θ = 20° and 0, 45, 90, 135, 180 and 270° with the detector at θ = 50°).

X-ray powder diffraction data were collected for the sample described in [8] on a parallel-beam Bruker AXS D8 Advance operating in transmission mode in θ/θ geometry. The instrument is equipped with a PSD VÅNTEC-1 and radial Soller on the diffracted beam. A fragment of the same crystal used for HRTEM was crushed in an agate mortar and the resulting powder was filled in a 0.3 mm diameter capillary. Data were collected in step scan mode in the 4-145° 2θ angular range, with a step size of

0.022° 2θ and 3 s of counting time. The low limit of 4° 2θ was chosen to avoid PSD damage from the incoming direct beam.

2.3. EMPA

Electron MicroProbe Analysis (EMPA) of the second crystal of sacrofanite was carried out on a Cameca SX50 electron microprobe under the following experimental conditions: 10 s counting time (peak), 10 s counting time (background), beam diameter 10 μm, excitation voltage 15 kV, specimen current 15 nA, wavelength-dispersive spectrometry (WDS). The following standards were used: wollastonite (Si and Ca), corundum (Al), orthoclase (K), jadeite (Na), barite (S), sylvite (Cl), and fluorophlogopite (F). The raw data were corrected on-line for drift, dead time, and background; matrix correction has been performed with a standard ZAF program. The unit formula was normalized on the basis of 12 (Si+Al). Chemical data are reported in Table 2. The two sacrofanite samples show minor differences at the chemical level that are mainly related to the increased Na content of the new crystal at the expenses of K. The low cation total of 7.8 atoms instead of expected 8, based on 12 (Si+Al), may be reasonably due to sodium loss during the analysis. A possible F loss could be also expected.

2.4. Structural refinements

The topological symmetry of the framework, as obtained by the electron microscopy analysis, is $P6_3/mmc$. However, crystal chemical considerations, as well as comparison with other phases of the group, point to an ordered distribution of Si and Al on the tetrahedral sites, which reduces the symmetry at least to $P\bar{6}2c$ (topochemical symmetry). The other space group suggested by the HRTEM study, namely $P6_3mc$,

does not allow an Al,Si ordering on the tetrahedral sites of the framework.. Therefore, the structural refinement started in space group $P\bar{6}2c$, introducing the tetrahedral atoms in their approximated positions, obtained from the stacking sequence |12(8)21|12(8)21|, that we deduced from the HRTEM photographs. By using the first data set (synchrotron radiation), these positions were refined in several cycles of full-matrix least-square refinement with the SHELXL program [20], whereas successive Fourier maps allowed for the extraframework cations and anion groups to be located within the different cages. Finally, all the oxygen atoms of the framework were localised. The average T-O distances were <Si-O> = 1.60(2) Å and <Al-O> = 1.72(2) Å, where the digits in parentheses refer to the actual dispersion of all the refined interatomic distances. The electron densities within the different cages were attributed to Na, K, and Ca cations (M sites), sulphur atoms, chlorine and fluorine anions and H_2O molecules on the basis of their height in the Fourier maps, their multiplicity, and crystal chemical considerations. The structural refinement, with anisotropic displacement parameters for Si, Al and for the extraframework cations not distributed over split atomic sites, converged up to R = 0.083 for 4,228 unique reflections. Furthermore, the refinement revealed the crystal to be twinned with [100] as twin axis, and 37% of twinning fraction.

This refined atomic coordinates were used as a starting model for the successive refinement, carried out by using the second intensity data set, collected up to a resolution of 0.62 Å. Also the second crystal was twinned with [100] as twin axis, the refined fraction of twinning being 47%. The higher number of available reflections allowed us to refine the anisotropic displacement parameters of all the framework atoms (Si, Al and O), as well as of the extraframework cations Na, Ca, and K not affected by positional disorder. The positions of the other cations, distributed over two or three split

sites, of the extraframework anions and of the H_2O molecules, were refined using isotropic displacement parameters. The refinement converged to $R = 0.090$ for 14,404 reflections with $F_o > 4\sigma(F_o)$, and to $R = 0.096$ for all the 15,795 reflections. Weak additional electron density maxima were found in the Differences Fourier Map, at distances less than 0.5 Å from some split sites of extraframework cations within the sodalite cages, indicating a higher degree of disorder within these cages.

The results of the two structural refinements are very similar, with the latter refinement showing a better accuracy. Information about the data collections and the structural refinements are listed in Table 3. Table 4, with the atomic positions and equivalent or isotropic displacement parameters, Tables 5, with the anisotropic displacement parameters, and the CIF files containing the full structural data from the two refinements are deposited. Table 6 reports a list of selected bond distances.

Whereas in the refinement of the synchrotron data the occupancies of the extraframework sites were fixed on the basis of the chemical analysis and of crystal chemical considerations, in the latter the occupancy factors of most M sites were allowed to vary during the refinement, applying the scattering factor of Ca. The only exceptions were M3 (fully occupied by Na) and the occupancies of the sites M15 and M16, which were refined using the scattering factor of K. By assuming that all the M sites (or groups of split M sites) were actually fully occupied, it was possible to calculate the Na : Ca (or Na : K) ratio. The results of these calculations are reported in Table 7, which lists the refined content of the different sites or groups of sites, and the ideal chemical content to assure a charge balanced chemical formula. The obtained site populations revealed the crystal chemical formula

$(Na_{61}K_{19}Ca_{32})_{\Sigma=112}(Si_{84}Al_{84}O_{336})(SO_4)_{26}Cl_2F_6 \cdot 2H_2O$, or

$(Na_{4.36}K_{1.36}Ca_{2.28})_{\Sigma=8.00}(Si_6Al_6O_{24})(SO_4)_{1.86}Cl_{0.14}F_{0.43} \cdot 0.14H_2O$ on the basis of 12 (Si+Al) atoms, which is in good agreement with the present and reference chemical data (Table 2). The recalculated water content is of approximately 0.25 wt%.

Structural data from the single-crystal analysis were used for fitting the powder diffraction data by the Rietveld method using the GSAS crystallographic suite of programs and the EXPGUI graphical user interface [21,22]. Because of strong correlations among structural parameters, only cell parameters and peak shape were refined. Nevertheless, the fitting was excellent. The refined unit cell parameters were a = 12.89609(12) Å, c = 74.2294(10), V = 10691.1(2) $Å^3$, in good agreement with the single crystal data. Final conventional disagreement indices were wR_p = 3.18%, R_p = 2.16%, R_{F2} = 5.47%. Rietveld plot is reported in Fig. 2.

3. Description of the structure

The framework of sacrofanite is schematically shown in Fig. 3. In accordance with the crystal chemistry of this supergroup of minerals (Table 1), and on the basis of the observed <T-O> distances for Si and Al-centred tetrahedra (Table 6), it is possible to state that Si and Al regularly alternate on the T sites. The different cages formed by the stacking of the layers will be described separately, by comparing them with similar cages occurring in other members of the supergroup.

3.1 Liottite cages

Two symmetry equivalent liottite cages, denoted as $[4^66^{17}]$ in the IUPAC nomenclature [23], are present along [1/3, 2/3, *z*], and [2/3, 1/3, *z*], respectively. This kind of cage was previously found and described in detail in liottite [24]; among the members of the supergroup, it occurs also in afghanite and alloriite, tounkite,

marinellite, farneseite, biachellaite, as well as in the 'ten-layer' and '18-layer' phases (Table 1). In all these phases, as well as in sacrofanite, the chemical content of this cage is very similar. There are three sulphate groups, which can display an orientational disorder, surrounded by three small cations (Na^+, partly substituted by Ca^{2+}). Three larger cations (namely K^+) are located in levels intermediate between two $(SO_4)^{2-}$ groups. The centres of the basal 6-ring of the cage are occupied by calcium cations. The shape of the cage is outlined in Fig. 3c, whereas its content is shown in Fig. 4.

3.2 Losod cages

Four symmetry related [$4^6 6^{11}$] cages (also known as 'losod cages') occur in sacrofanite; two of them are located along [1/3, 2/3, *z*], and the other along [2/3, 1/3, *z*], respectively. The couples of cages are separated by a smaller cage, namely a 'cancrinite cage' [$4^6 6^5$]. Also the losod cage occurs in many members of the supergroup: besides the synthetic 'losod' and the isostructural minerals bystrite and carbobystrite, it occurs also in liottite, franzinite, tounkite, '18-layer phase' and in the phases with very long sequences of layers (biachellaite, fantappiéite, kircherite, and obviously sacrofanite). In sacrofanite, the losod cage contains two (SO_4) groups, aligned along the three-fold axis and not affected by positional disorder (Fig. 5). Triples of symmetry equivalent sites M10 and M11, containing Na^+ and Ca^{2+} cations, are located around each (SO_4) group, respectively, whereas in the layer between them three larger K^+ cations are located, with minor Na^+ substitution.

3.3 Sodalite cages

The stacking sequence of the layers in the sacrofanite structure gives rise to two groups of six sodalite cages [$4^6 6^8$] per unit cell, connected as shown in Fig. 6. All the

sodalite cages show a high degree of disorder, both chemical and positional. This situation is common in all the minerals of the supergroup showing this type of cage, usually containing sulphate groups in more than one orientation, as well as split M sites that may host Na^{+} or Ca^{2+} cations.

3.4 Cancrinite cages

Eight of the ten cancrinite cages in the structure of sacrofanite are located along [0, 0, *z*] (Fig. 7a). They contain H_2O or fluorine anions, as indicated by the chemical data (Table 2) and by the electron densities within the cages. The two remaining cancrinite cages are located along [1/3, 2/3, *z*] and [2/3, 1/3, *z*], respectively, between the two losod cages previously described (Fig. 7b). Each of them hosts a chlorine anion, which is sensibly displaced from the symmetry axis to form a convenient bond distance with M8, M8b, M8c sites, occupied by Na^{+} cations.

4. Conclusions

The crystal structure of sacrofanite was solved and refined by using different techniques and sources of data. The structural results are in agreement with the crystal chemistry of the cancrinite-sodalite supergroup, which comprises 36 official minerals with stacking sequences ranging from 2 to 36 layers and *c* parameters ranging from 5 to 95 Å.

The occurrence of phases with so large unit cells, such as sacrofanite and other members of the cancrinite-sodalite supergroup, raises the question of their stability field, with respect to possible more simple stacking sequences. Because minerals with a different stacking sequence may be found in the same paragenesis, often in the same hand sample (*e.g.* marinellite and giuseppettite [25, 26]) and, in some occasions, also in

the same ‘crystal’ [27], it seems unlikely that temperature and/or pressure may play a significant role to stabilise a particular long periodicity with respect to others. However, each different stacking sequence corresponds to a different number of cage types, which exhibit an affinity to host certain anionic groups, such as $(SO_4)^{2-}$, the anions Cl^- and F^-, or water molecules. The sulphate groups may be hosted in the sodalite cages (1 SO_4), losod cages (2 SO_4), liottite cages (3 SO_4) and giuseppettite cages (4 SO_4), whereas they cannot enter into the small cancrinite cages. On the contrary, such small cages may host anions Cl^- and F^-, as well as H_2O molecules. Based on these considerations, an ideal anionic content may be evaluated for each stacking sequence. The differences in the ideal chemical compositions may be appreciated in the plot of the maximum sulphate content *versus* the amount of (Cl,F,H_2O) in the cancrinite cages, drawn in Fig. 9 of [1]. The minerals showing ABC... stacking sequence (‘sodalite group’), ABAB... stacking sequence (‘cancrinite group’), and the phases with more complex sequences of layers occupy well-separated fields in this graph. Moreover, the points corresponding to these last phases are aligned in two different trends. The right comprises phases characterised by the absence of sodalite cages, and the left includes sacrofanite and other phases which present several sodalite cages in their structure. The most recent version of the diagram, showing only the phases with complex sequences of layers, is shown in Fig. 8.

The knowledge of the crystal chemistry of this supergroup of minerals could help in solving new unknown structures, by greatly reducing the number of their possible stacking sequences on the basis of the amount and type of extra-framework anions and hence of the amount and type of structural cages.

Acknowledgments

We warmly thank F. Bellatreccia, who provided us with one of the samples of sacrofanite for study. This research was financially supported by MIUR through project PRIN 2007 "Compositional and structural complexity in minerals (crystal chemistry, microstructures, modularity, modulations): analysis and applications", by Sapienza University of Roma, and by the CNR project TA.01.004.002. EMPA was carried out at CNR-IGAG under the supervision of M. Serracino, HRTEM at the Arizona State University Center for High-resolution Electron Microscopy. Thank are due to P.R. Buseck and A. Maras for an early stay of P.B. at Arizona State University. Finally, we are grateful to the referees for improving the paper with useful suggestions and criticisms.

References

[1] E. Bonaccorsi, S. Merlino, Rev. Mineral. Geochem. 57 (2005) 241.

[2] W.H. Baur , R.X. Fischer (Eds.), Microporous and other framework materials with zeolite-type structures. Springer-Verlag, Berlin, Heidelberg, 2000.

[3] H. Gies, R. Kirchner, H. van Koningsveld, M.M.J. Treacey, in: M.M.J. Treacey, B.K. Marcus, M.E. Bisher, J.B. Higgins (Eds.), Proc. 12th International Zeolite Conference, Materials Research Society, MRS, Warrendale, Pennsylvania, 1999, pp. 2999-3029.

[4] S.J. Mills, F. Hatert, E.H. Nickel, G. Ferraris G., Eur. J. Mineral. 21 (2009) 1073.

[5] R.K. Rastsvetaeva, A.G. Ivanova, N.V. Chukanov, I.A. Verin, Dokl. Earth Sci. 415 (2007) 815.

[6] A.P. Khomyakhov, F. Cámara, E. Sokolova, Can. Mineral. 48 (2010) 291.

[7] R.K. Rastvetaeva, N.V. Chukanov, A.G. Ivanova, Crystallogr. Rep. 54 (2009) 195.

[8] F. Burragato, G.C. Parodi, P.F. Zanazzi, Neues. Jb. Miner. Abh. 140 (1980) 102.

[9] P. Ballirano, A. Maras, P.R. Buseck, S. Wang, A.M. Yates, Powder Diffr. 10 (1995) 13.

[10] N.V.Chukanov, R.K. Rastsvetaeva, I.V. Pekov, A.E. Zadov, R. Allori, N.V. Zubkova, G. Giester, D.Yu. Puscharovsky, K.V. Van, Geol. Ore Deposits 51 (2009) 588.

[11] F. Camara, F. Bellatreccia, G. Della Ventura, A. Mottana, L. Bindi, M.E. Gunter, M. Sebastiani, Am. Mineral. 95 (2010) 472.

[12] P. Ballirano, Plinius 11 (1994) 81.

[13] F. Bellatreccia, F. Cámara, G. Della Ventura, M.E. Gunter, A. Cavallo, M. Sebastiani, Acta Mineralogica-Petrographica, Abstract series 6 (2010) 493.

[14] P. Ballirano, E. Bonaccorsi, Acta Crystallogr. A61 (2005) c382.

[15] R. Henderson, P.N.T. Unwin, Nature 257 (1975) 28.

[16] S. Hovmöller, Ultramicroscopy 41 (1992) 121.

[17] P. Ballirano, A. Maras, P.R. Buseck, Am. Mineral. 81 (1996) 1003.

[18] Z. Otwinowski, W. Minor, in: C.W. Carter, Jr., R.M. Sweet (Eds.), Methods in Enzymology, Volume 276: Macromolecular Crystallography, part A, Academic Press, 1997 pp. 307-326.

[19] G.M. Sheldrick, SADABS UserGuide (1998) University of Göttingen, Germany

[20] G.M. Sheldrick, Acta Crystallogr. A64 (2008) 112.

[21] A.C. Larson, R.B. Von Dreele, GSAS: General Structure Analysis System. LAUR 86-748, Los Alamos National Laboratory, Copyright, 1985-1994, The Regent of the University of California.

[22] B.H. Toby, J. Appl. Crystallogr. 34 (2001) 210.

[23] L.B. McCusker, F. Liebau, G. Engelhardt, Pure Appl. Chem. 73 (2001) 381.

[24] P. Ballirano, S. Merlino, E. Bonaccorsi, A. Maras, Can. Mineral. 34 (1996) 1021.

[25] E. Bonaccorsi, P. Orlandi, Eur. J. Mineral. 15 (2003) 1019.

[26] E. Bonaccorsi, Micropor. Mesopor. Mat. 73 (2004) 129.

[27] R. Rinaldi, H.-R. Wenk, Acta Crystallogr. A35 (1979) 825.

Table 1. Classification of the cancrinite-sodalite supergroup. The three capital letters in parenthesis are the framework type codes, assigned by the Structure Commission of the International Zeolite Association to the unique and confirmed framework topologies.

Cancrinite group (CAN)	Sodalite group (SOD)	Bystrite group (LOS)	Afghanite group (AFG)	Unassigned members of the sodalite-cancrinite supergroup
cancrinite	sodalite	bystrite	afghanite	liottite (LIO)
vishnevite	haüyne	carbobystrite	alloriite	franzinite (FRA)
hydroxycancrinite	nosean	'losod' (synth.)		"ten-layer phase" (*)
cancrisilite	lazurite			tounkite (TOL)
kyanoxalite	helvite			marinellite (MAR)
pitiglianoite	genthelvite			farneseite (FAR)
depmeierite	danalite			giuseppettite (GIU)
davyne	bicchulite			"18-layer phase" (**)
microsommite	tugtupite			sacrofanite
quadridavyne	tsaregorodsevite			biachellaite
balliranoite				fantappiéite
tiptopite				kircherite

(*) It is not a CNMNC approved mineral [6].
(**) Unpublished results.

Table 2. Chemical analysis and unit formula, calculated on the basis of 12(Si+Al), for sacrofanite. a) Reference chemical data of Ballirano et al. (1995); b) present work. Average over 20 analytical points. The unit formula from reference data has been recalculated.

	a	*b*		*a*	*b*
SiO_2	30.72	31.26	Si	6.04	6.00
Al_2O_3	25.75	26.53	Al	5.96	6.00
			$\Sigma_{(Si+Al)}$	12	12
CaO	10.98	11.47	Ca	2.31	2.36
Na_2O	9.84	10.56	Na	3.75	3.93
K_2O	6.60	6.15	K	1.65	1.51
			Σ_{cat}	7.71	7.80
SO_3	12.48	12.81	SO_4	1.84	1.85
Cl	0.50	0.45	Cl	0.17	0.15
F	0.47	0.56	F	0.29	0.34
	97.36	99.79			
O=Cl,F	-0.31	-0.34	O	23.96	23.99
Total	97.05	99.45			

Table 3. Crystal data and structure refinements for the two crystals of sacrofanite. The central column refers to the synchrotron data collection, whereas the last one refers to the data collected for a larger crystal with a laboratory diffractometer.

Chemical formula	$(Na_{62}K_{18}Ca_{32})_{\Sigma=112}(Si_{84}Al_{84}O_{336})(SO_4)_{26}Cl_2(F,OH)_6 \cdot 2H_2O$	
Wavelength	1.0 Å	0.71069 Å
Crystal system	hexagonal	
Space group	$P\bar{6}2c$	
Unit cell dimensions	a = 12.903(2) Å	a = 12.8857(5) Å
	c = 74.284(8) Å	c = 74.192(3) Å
Volume	10710(2) Å^3	10668.5(8) Å^3
Z	1	
Crystal size	0.1 × 0.1 × 0.2 mm^3	0.70 × 0.63 × 0.52 mm^3
Theta range for data collection	2.59 to 31.41°.	0.82 to 35.03°.
Index ranges	$-13 \le h \le 13$	$-20 \le h \le 20$
	$-13 \le k \le 13$	$-20 \le k \le 20$
	$-77 \le l \le 77$	$-115 \le l \le 119$
Reflections collected	78202	243251
Independent reflections	4,228 [R_{int} = 0.0353]	15,795 [R_{int} = 0.0407]
Completeness	(to theta = 25°) 95.6 %	99.8 %
Refinement method	Full-matrix least-squares on F^2	
Data / restraints / parameters	4,228 / 0 / 469	15,795 / 4 / 622
Goodness-of-fit on F^2	1.113	1.084
Final R indices [$I > 2\sigma(I)$]	$R1$ = 0.0825	$R1$ = 0.0903
	$wR2$ = 0.2399	$wR2$ = 0.2821
R indices (all data)	$R1$ = 0.0827	$R1$ = 0.0960
	$wR2$ = 0.2402	$wR2$ = 0.2887
Largest diff. peak and hole	1.213 and -1.015 e.Å^{-3}	2.015 and -2.786 e.Å^{-3}

Table 6. Selected bond distances for sacrofanite as determined from the laboratory diffractometer data.

Si1-O1	1.618(12)	Si2-O4	1.560(6)	Si3-O22	1.601(4)	Si4-O17	1.595(5)
-O1	1.618(12)	-O7	1.568(8)	-O9	1.605(4)	-O23	1.598(5)
-O3	1.595(4)	-O8	1.583(8)	-O20	1.612(5)	-O21	1.602(4)
-O3	1.595(4)	-O13	1.587(6)	-O12	1.620(5)	-O24	1.608(5)
average	1.606	average	1.575	average	1.610	average	1.601
Si5-O18	1.601(5)	Si6-O27	1.585(5)	Si7-O29	1.601(4)	Si8-O2	1.597(7)
-O16	1.602(4)	-O26	1.605(4)	-O10	1.609(4)	-O11	1.626(6)
-O19	1.604(4)	-O28	1.609(4)	-O25	1.611(4)	-O6	1.626(4)
-O14	1.625(5)	-O15	1.635(4)	-O5	1.628(4)	-O6	1.626(4)
average	1.608	average	1.608	average	1.612	average	1.619
Al1-O1	1.731(13)	Al2-O8	1.680(8)	Al3-O22	1.704(4)	Al4-O24	1.709(6)
-O1	1.731(13)	-O3	1.701(5)	-O13	1.706(7)	-O16	1.723(4)
-O4	1.680(6)	-O12	1.701(5)	-O21	1.707(5)	-O20	1.731(5)
-O4	1.680(6)	-O7	1.703(8)	-O9	1.716(5)	-O23	1.734(5)
average	1.706	average	1.696	average	1.708	average	1.724
Al5-O15	1.713(5)	Al6-O28	1.706(4)	Al7-O26	1.718(4)	Al8-O11	1.690(6)
-O17	1.726(5)	-O27	1.734(5)	-O10	1.719(4)	-O2	1.698(7)
-O19	1.726(4)	-O14	1.744(5)	-O6	1.728(4)	-O5	1.751(4)
-O18	1.738(5)	-O25	1.751(4)	-O29	1.743(4)	-O5	1.751(4)
average	1.726	average	1.734	average	1.727	average	1.723
M1-O1A	2.60(3)	M2-O24	2.449(6)	M2B-O1C	2.42(3)	M2C-O1D	2.29(7)
-O1A	2.60(3)	-O24	2.449(6)	-O1C	2.42(3)	-O24	2.389(4)
-O1A	2.60(3)	-O1C	2.83(3)	-O1C	2.42(3)	-O24	2.389(4)
M1B-O1B	2.65(5)	-O1C	2.83(3)	-O24	2.596(10)	-F3	2.55(3)
-O1B	2.65(5)	-O1C	2.83(3)	-O24	2.596(10)	-F3	2.55(3)
-O1	2.913(10)	-O23	2.854(4)	-O23	2.931(7)	-F3	2.55(3)
-O1	2.913(10)	-O23	2.854(4)			-O23	2.856(4)
		-F3	3.02(3)			-O23	2.856(4)
		-F3	3.02(3)				
M3-F3	2.22(3)	M3B-O27	2.618(4)	M4-O11	2.564(4)	M4B-F1	2.10(2)
-F3	2.22(3)	-O27	2.618(4)	-O11	2.564(4)	-F1	2.10(2)
-F3	2.22(3)	-F1	2.695(17)	-O11	2.564(4)	-O11	2.644(6)
-O28	2.721(4)	-F1	2.695(17)	-O2	2.728(5)	-O11	2.644(6)
-O28	2.721(4)	-O28	2.727(4)	-O2	2.728(5)	-O11	2.644(6)

-O27	2.734(8)	-O28	2.727(4)	-F1	2.735(12)	-O2	2.803(6)
-O27	2.734(8)	-F3	2.82(2)	-F1	2.735(12)	-O2	2.803(6)
		-F3	2.82(2)	-F1	2.735(12)		
M5-O6A	2.18(3)	M5B-O22	2.502(5)	M6-O6F	2.30(4)	M6B-O7D	2.13(6)
-O3A	2.269(16)	-O22	2.502(5)	-O6F	2.30(4)	-O8	2.582(8)
-O6E	2.35(4)	-O22	2.502(5)	-O6F	2.30(4)	-O8	2.582(8)
-O6E	2.35(4)	-O6A	2.57(3)	-O8	2.676(10)	-O7C	2.79(2)
-O6E	2.35(4)	-O6E	2.71(4)	-O8	2.676(10)	-O7C	2.79(2)
-O22	2.552(5)	-O6E	2.71(4)	-O6B	2.67(2)	-O7C	2.79(2)
-O22	2.552(5)	-O6E	2.71(4)	-O6B	2.67(2)		
-O22	2.552(5)	-O9	2.710(6)	-O6B	2.67(2)		
-O9	2.698(6)	-O9	2.710(6)	-O7	2.851(7)		
-O9	2.698(6)	-O9	2.710(6)	-O7	2.851(7)		
-O9	2.698(6)						
M7-O7A	2.05(12)	M8-Cl2	2.335(3)	M8B-O10	2.431(3)	M8C-O10	2.457(6)
-O4A	2.252(10)	-Cl2	2.335(3)	-O10	2.431(3)	-O10	2.457(6)
-O19	2.450(3)	-O5A	2.364(8)	-Cl2	2.744(17)	-O29	2.898(4)
-O19	2.450(3)	-O10	2.528(3)	-Cl2	2.744(17)	-O29	2.898(4)
-O7B	2.569(15)	-O10	2.528(3)	-O29	2.936(5)		
-O7B	2.569(15)	-O29	3.068(3)	-O29	2.936(5)		
-O7B	2.569(15)	-O29	3.068(3)				
-O18	2.854(4)						
-O18	2.854(4)						
M9-O6B	2.19(2)	M9B-O6F	2.34(7)	M10-O3B	2.329(6)	M11-O15	2.442(5)
-O7	2.493(10)	-O7	2.624(11)	-O21	2.533(8)	-O5B	2.459(5)
-O7	2.495(11)	-O6F	2.63(7)	-O18	2.617(4)	-O4B	2.475(5)
-O6B	2.61(2)	-O3	2.720(16)	-O17	2.633(6)	-O26	2.539(5)
-O3	2.615(12)	-S6	2.737(15)	-O7B	2.646(16)		
-O4	2.687(14)	-O7	2.738(12)				
-O4	2.734(14)	-O4	2.818(17)				
M12-Cl2	2.241(4)	M13-O12	2.451(18)	M13B-O23	2.650(8)	M13C-O7C	2.38(2)
-O2B	2.318(15)	-O13	2.518(18)	-O21	2.735(12)	-O1C	2.46(3)
-O2B	2.318(15)	-O23	2.564(11)	-O20	2.768(11)	-O23	2.452(5)
-O5	2.481(4)	-O21	2.852(17)	-O12	2.771(13)	-O12	2.480(10)
-O6	2.488(4)	-O20	2.928(17)	-O7D	2.785(7)	-O13	2.522(12)
-O6	2.488(4)			-O13	2.811(14)	-O21	2.661(9)
-O2A	2.592(18)					-O20	2.739(8)

-O2A	2.592(18)						
-O29	2.866(3)						
M14-O6C	2.23(6)	M14B –O1	2.373(15)	M15-O3	2.783(9)	M16-O2A	2.77(3)
-O1A	2.34(3)	-O6E	2.50(4)	-O3B	2.830(9)	-O4B	2.783(6)
-O1	2.273(10)	-O4	2.63(2)	-O5B	2.841(6)	-O5	2.783(4)
-O4	2.596(14)	-O13	2.83(2)	-O5B	2.857(7)	-O6	2.785(4)
-O13	2.703(12)	–O1	2.436(11)	-O17	2.866(5)	-O2A	2.79(3)
		-O13	2.780(14)	-O15	2.953(5)	-O4B	2.852(6)
		-O1B	2.805(10)	-O28	3.045(4)	-O26	2.953(5)
		-O4	2.823(17)				
S1-O1C	1.32(3)			S3-O3B	1.461(6)	S4-O4A	1.454(10)
-O1A	1.32(3)	S2-O2B	1.342(15)	-O3B	1.461(6)	-O4B	1.476(4)
-O1D	1.45(7)	-O2B	1.342(14)	-O3B	1.461(6)	-O4B	1.476(4)
-O1B	1.51(5)	-O2B	1.342(15)	-O3A	1.473(15)	-O4B	1.476(4)
-O1C	1.61(4)	-O2B	1.342(14)				
-O1A	1.63(4)	-O2B	1.342(14)	S6-O6F	1.42(4)	S7-O7D	1.22(6)
-O1A	1.78(4)	-O2B	1.342(14)	-O6F	1.40(5)	-O7B	1.307(16)
-O1C	1.82(3)	-O2A	1.628(18)	-O6B	1.43(3)	-O7C	1.31(2)
		-O2A	1.628(18)	-O6E	1.43(4)	-O7C	1.68(2)
S5-O5A	1.452(8)	-O2A	1.628(18)	-O6C	1.51(6)	-O7B	1.711(18)
-O5B	1.474(5)	-O2A	1.628(18)	-O6B	1.60(3)	-O7B	1.943(17)
-O5B	1.474(5)	-O2A	1.628(18)	-O6E	1.61(4)	-O7C	1.96(2)
-O5B	1.474(4)	-O2A	1.628(18)				

Table 7. Site population in sacrofanite as determined from the laboratory diffractometer data. The partial site occupancies were obtained on the basis of the scattering power of Ca, except for M3-M3B (Na) and M15-M16 (K). The last three columns list the idealized cationic content of each site or group of sites, to obtain a charge balanced formula.

	Partial occupancy	Number of electrons	%Na	%Ca	%K	Mult.	Na	Ca	K	Ideal Na	Ideal Ca	Ideal K
M1 M1B	0.532 0.100	12.64	82	18	0	2*	1.64	0.36	0	1.5	0.5	0
M2 M2B M2C	0.288 0.170 0.232	13.80	69	31	0	4*	2.76	1.24	0	3	1	0
M3 M3B	0.328 0.672	11.00	100	0	0	4*	4.00	0.00	0	4	0	0
M4 M4B	0.541 0.274	16.30	41	59	0	2*	0.82	1.18	0	1	1	0
M5 M5B	0.711 0.165	17.52	28	72	0	4*	1.10	2.90	0	1.5	2.5	0
M6 M6B	0.356 0.253	12.17	87	13	0	4*	3.48	0.52	0	3.5	0.5	0
M7	1.000	20.00	0	100	0	4	0.00	4.00	0	0	4	0
M8 M8B M8C	0.906 0.046 0.042	19.87	1	99	0	4*	0.06	3.94	0	0	4	0
M9 M9B	0.407 0.280	13.73	70	30	0	6*	4.18	1.82	0	4	2	0
M10	0.649	12.98	78	22	0	12	9.36	2.64	0	9.5	2.5	0
M11	0.798	15.97	45	55	0	12	5.38	6.62	0	5.5	6.5	0
M12	0.842	16.84	35	65	0	6	2.11	3.89	0	2.5	3.5	0
M13 M13B M13C	0.126 0.201 0.358	13.72	70	30	0	12*	8.38	3.62	0	9	3	0
M14 M14B M14C	0.305 0.122 0.181	12.16	87	13	0	12*	10.45	1.55	0	11	1	0
M15	0.900	17.10	24	0	76	12	2.86	0	9.14	3	0	9
M16	0.918	17.44	19	0	81	12	2.34	0	9.66	2	0	10

total	58.92	34.28	18.80	61	32	19

* Maximum cations number per group of sites because of mutual exclusion rules.

Figure captions

Fig. 1. HRTEM image of sacrofanite, zone axis [100].

Fig. 2. Experimental (dots) and calculated (continuous line) Rietveld plots for sacrofanite. The difference profile is shown at the bottom of the figure. Vertical markers refer to the position of the calculated Bragg reflections.

Fig. 3. Schematic drawing of the framework of sacrofanite, projected along [100]. In (a) the unit cell is outlined. For sake of simplicity, the cages that are superimposed along [0, 0, *z*], [1/3, 2/3, *z*], and [2/3, 1/3, *z*], are shown separately in (b), (c) and (d), respectively. *lio* = liottite cage [$4^6 6^{17}$]; *los* = losod cage [$4^6 6^{11}$]; *sod* = sodalite cage [$4^6 6^8$]; *can* = cancrinite cage [$4^6 6^5$].

Fig. 4. Liottite cage in sacrofanite. The S2-centred tetrahedron, with S2 placed on the mirror plane at $z = ¼$, may statistically assume different orientations. For sake of clarity, only one of them is shown.

Fig. 5. Losod cage in sacrofanite.

Fig. 6. . Sodalite cages in sacrofanite. All the possible orientations of the $(SO_4)^{2-}$ groups and all the split sites for the extra-framework cation are shown.

Fig. 7. Cancrinite cages in sacrofanite. In (a) the two symmetry-independent cancrinite cages located along the six-fold axis are shown. The F1 and F3 sites host fluorine anions, partially substituted by H_2O molecules. In (b) the cancrinite cage along each three-fold axis is sketched.

Fig. 8. Different compositional fields of the phases with a complex sequences of layers.

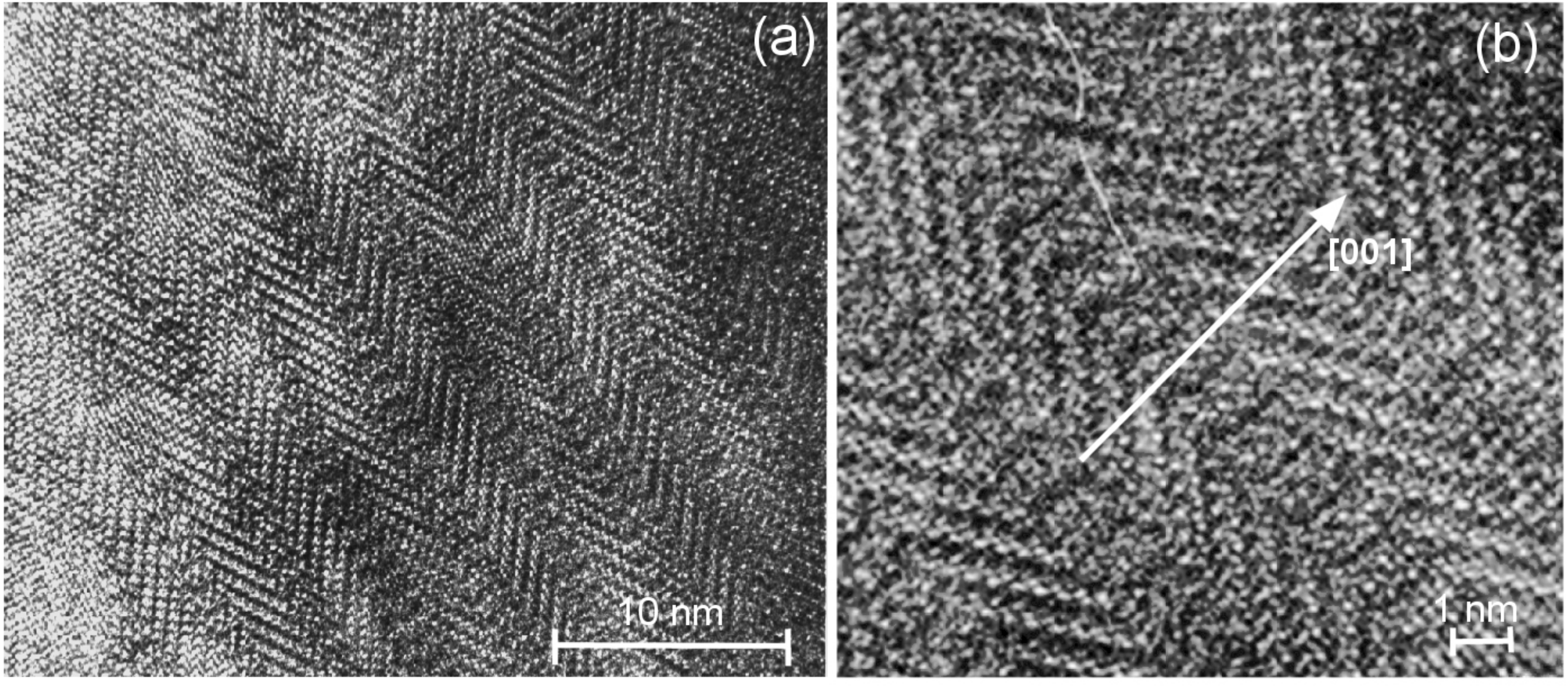
(a)
10 nm
(b)
[001]
1 nm

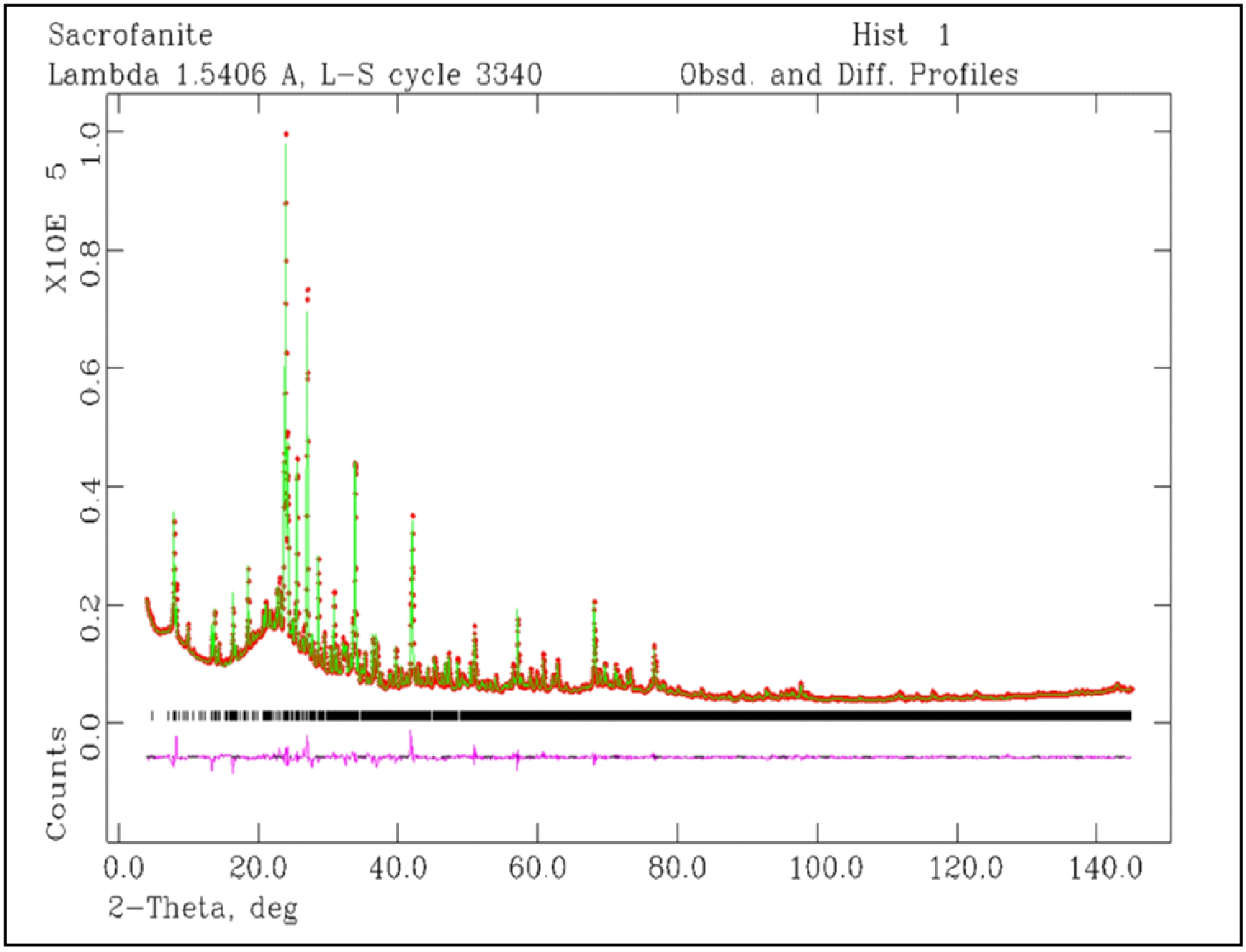
Sacrofanite
Hist 1
Lambda 1.5406 A, L-S cycle 3340
Obsd. and Diff. Profiles
X10E 5
1.0
0.8
0.6
0.4
0.2
0.0
Counts
0.0
20.0
40.0
60.0
80.0
100.0
120.0
140.0
2-Theta, deg

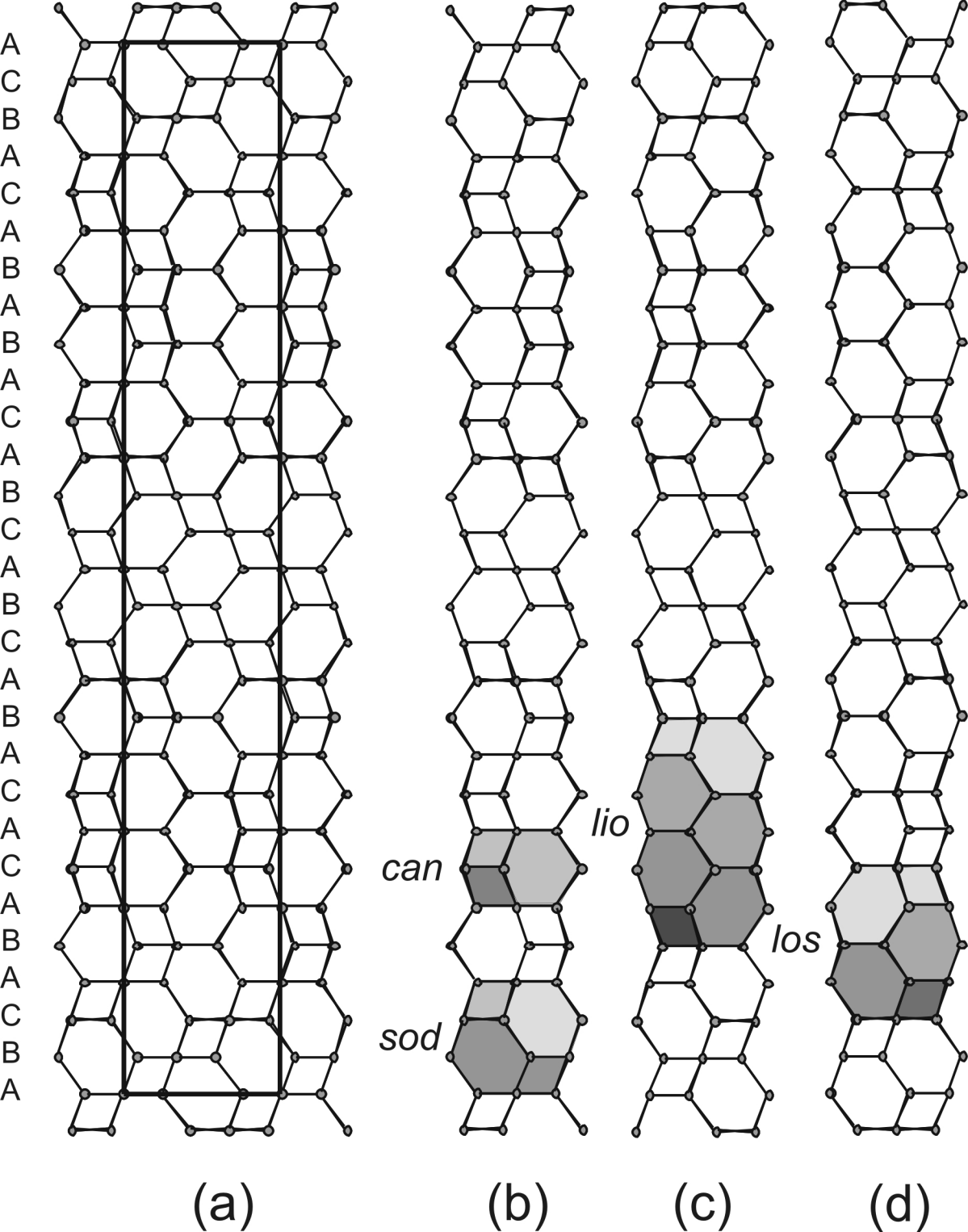
A
C
B
A
C
A
B
A
B
A
C
A
B
C
A
B
C
A
B
A
C
A
C
A
B
A
C
B
A
can
sod
lio
los
(a)
(b)
(c)
(d)

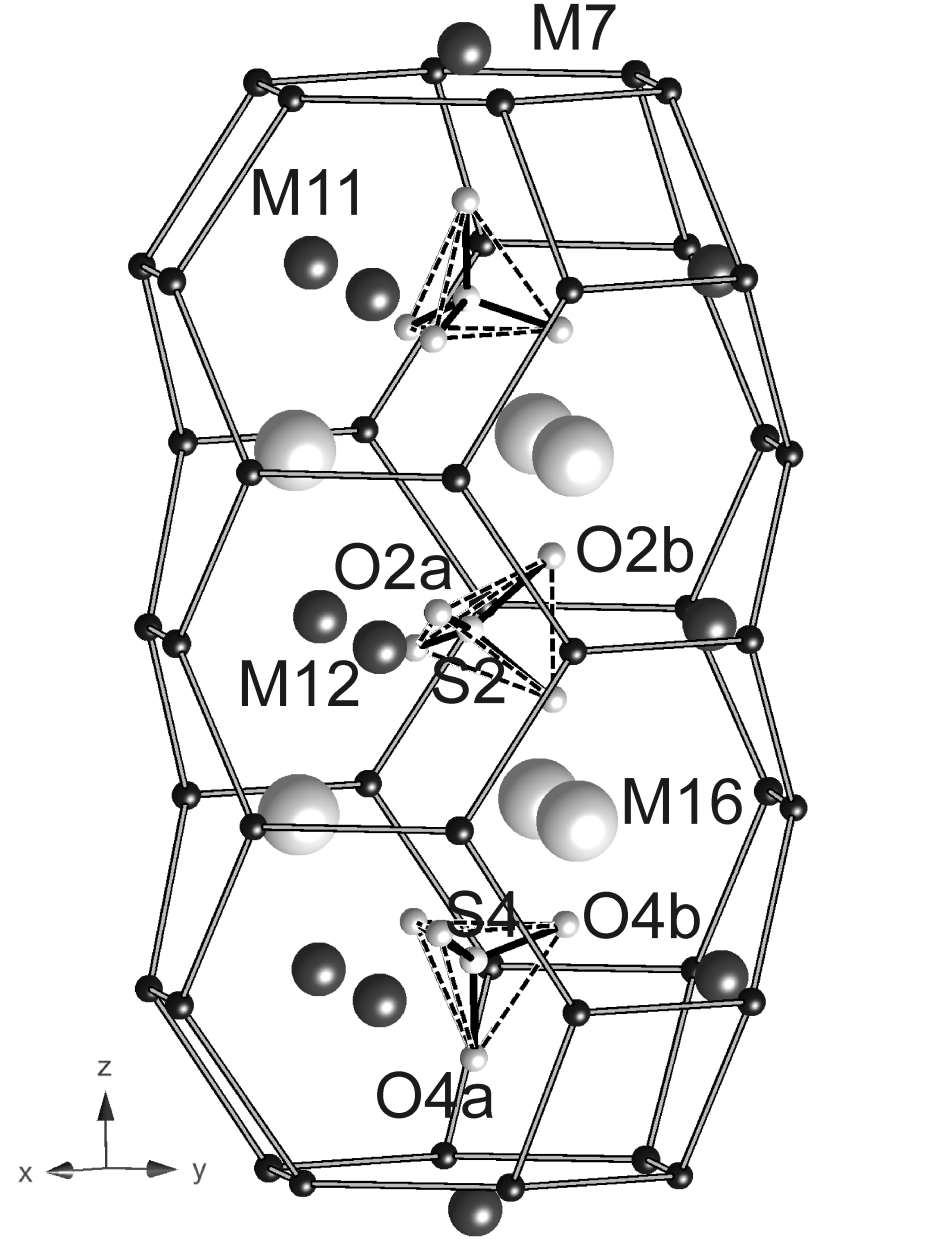
M7
M11
O2a
O2b
M12
S2
M16
S4
O4b
O4a
z
x
y

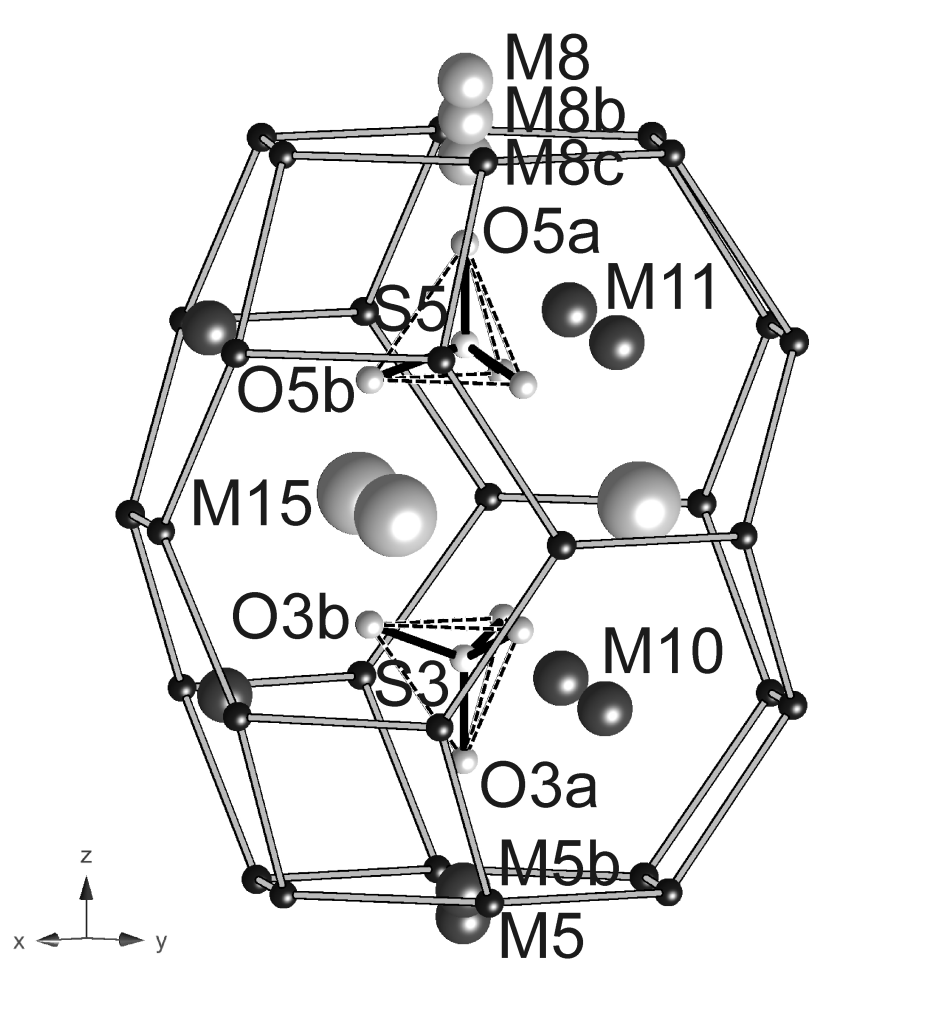
M8
M8b
M8c
O5a
M11
S5
O5b
M15
O3b
M10
S3
O3a
M5b
M5
z
x
y

(a)

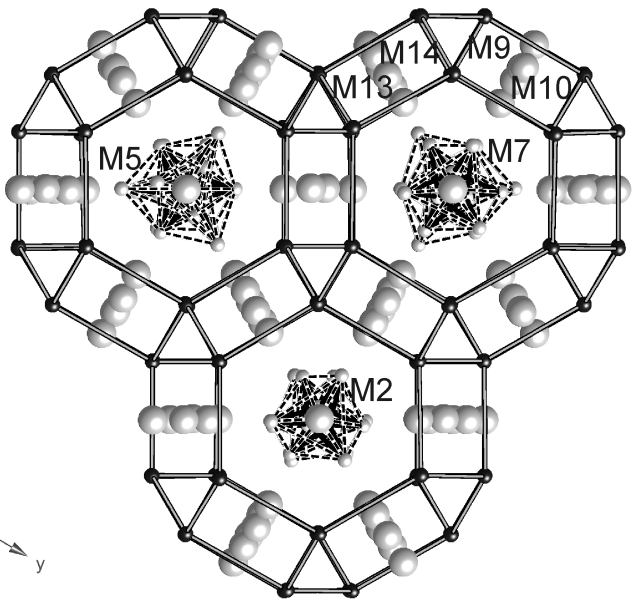

(b)

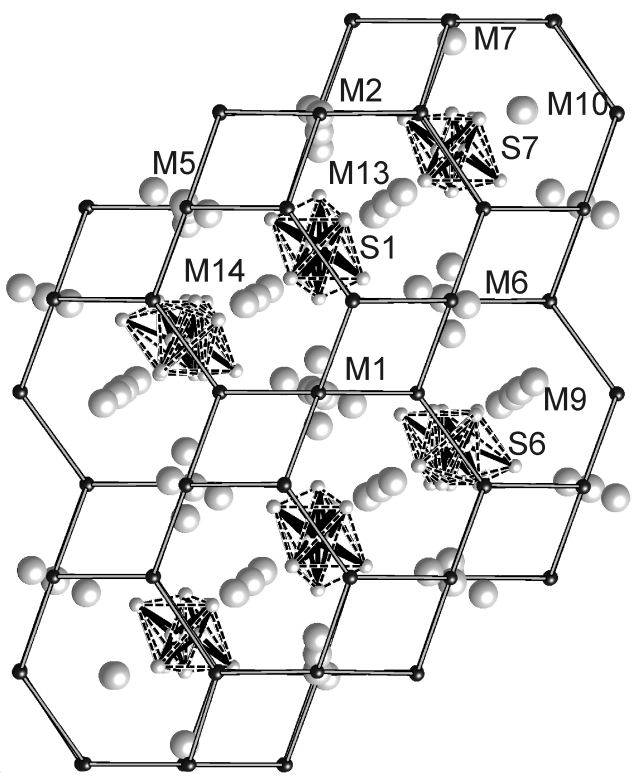

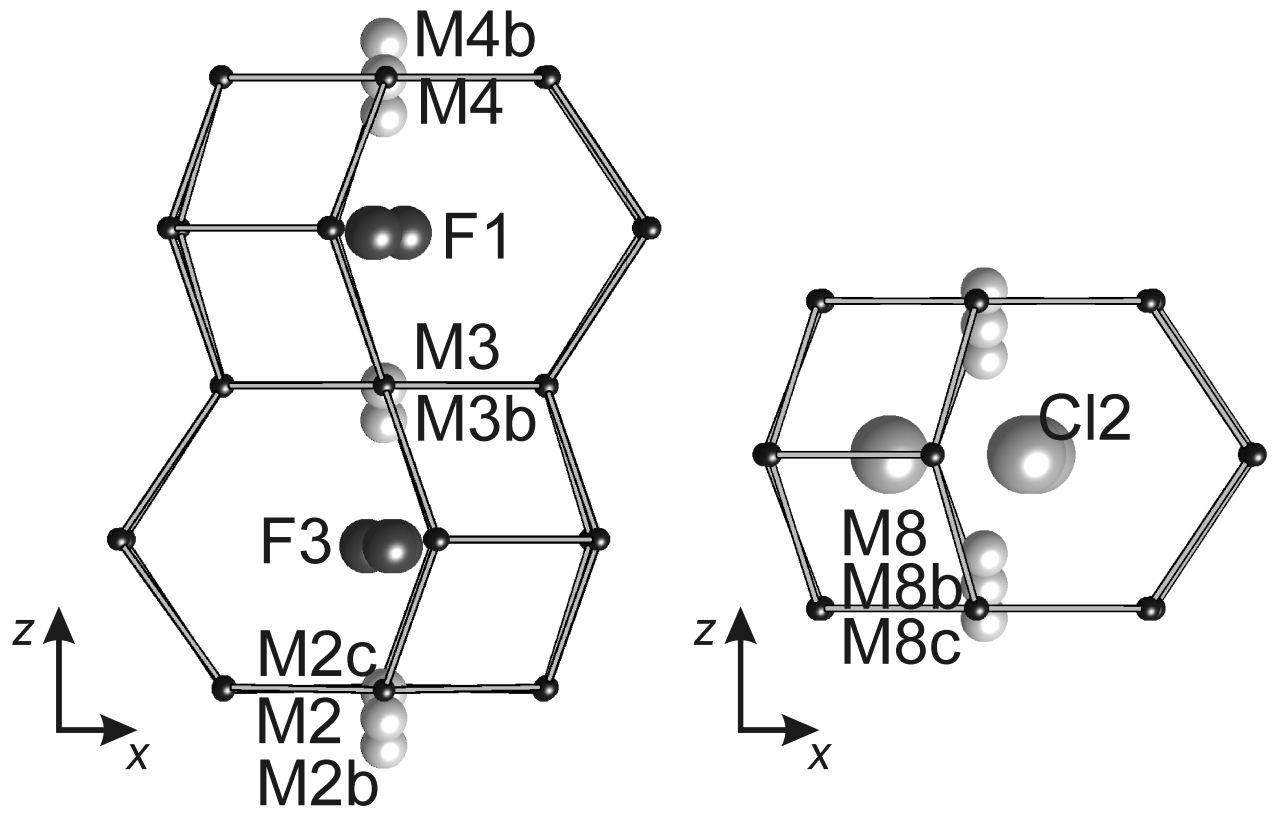

(a) (b)

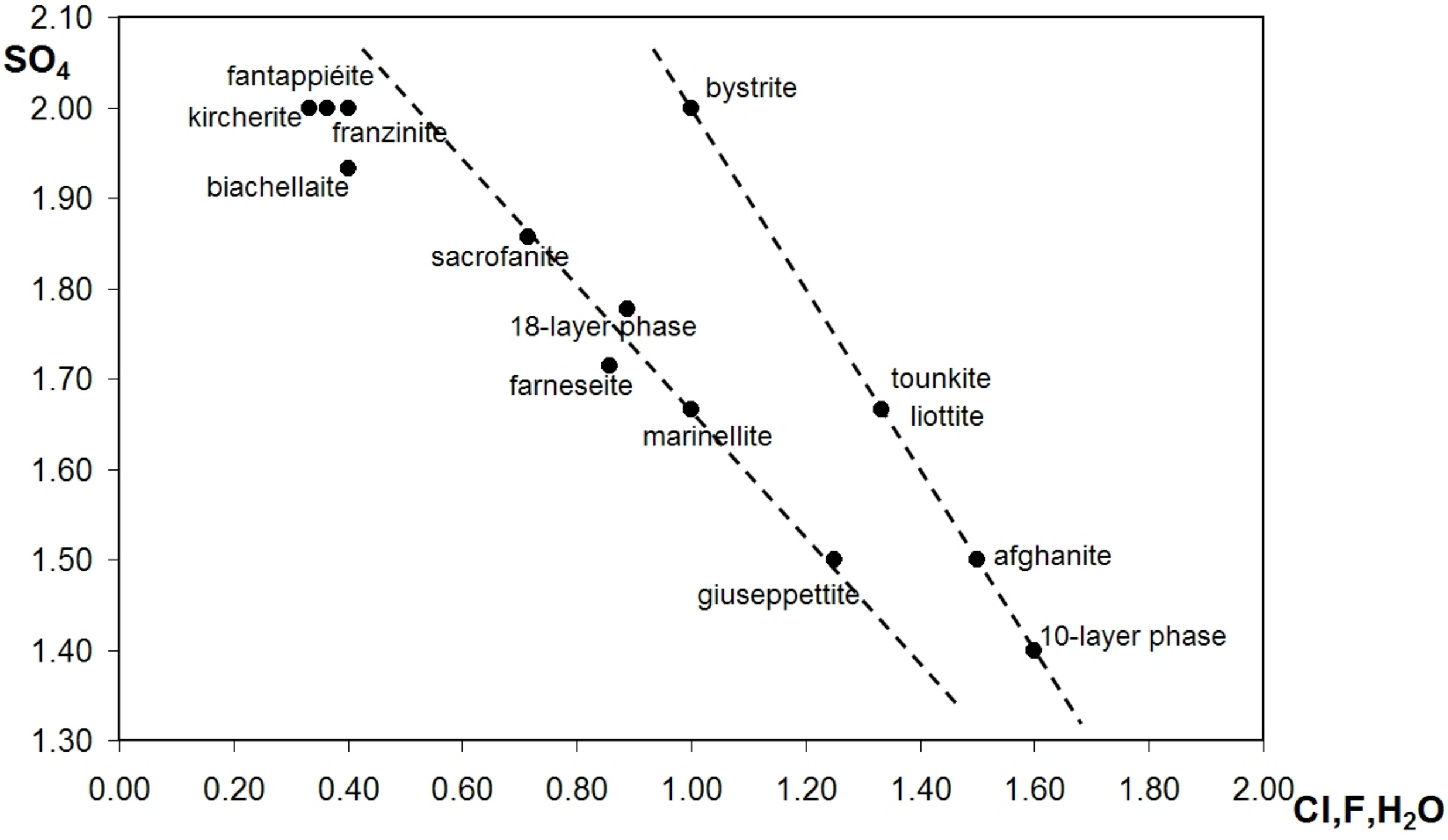
SO4
2.10
2.00
1.90
1.80
1.70
1.60
1.50
1.40
1.30
fantappiéite
kircherite
franzinite
biachellaite
sacrofanite
18-layer phase
farneseite
marinellite
giuseppettite
bystrite
tounkite
liottite
afghanite
10-layer phase
0.00
0.20
0.40
0.60
0.80
1.00
1.20
1.40
1.60
1.80
2.00
Cl,F,H2O